NASA TECHNICAL NOTE

NASA TN D-3717

NASA TN D-3717

THE NEAR-EARTH METEOROID ENVIRONMENT

by Robert J. Naumann

George C. Marshall Space Flight Center

Huntsville, Ala.

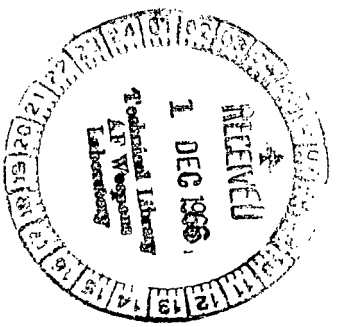

NATIONAL AERONAUTICS AND SPACE ADMINISTRATION • WASHINGTON, D. C. • NOVEMBER 1966

NASA TN D-3717

THE NEAR-EARTH METEOROID ENVIRONMENT

By Robert J. Naumann

George C. Marshall Space Flight Center
Huntsville, Ala.

NATIONAL AERONAUTICS AND SPACE ADMINISTRATION

For sale by the Clearinghouse for Federal Scientific and Technical Information
Springfield, Virginia 22151 – Price $2.00

TABLE OF CONTENTS

LIST OF ILLUSTRATIONS

LIST OF TABLES

THE NEAR-EARTH METEOROID ENVIRONMENT

By Robert J. Naumann

SUMMARY

A detailed study of the meteoroid environment has been completed utilizing observational data taken from Explorer XVI, Explorer XXIII, Pegasus I, II, and III, as well as from radar and photographic techniques. These observations cover the entire spectrum of masses important to the meteoroid hazard problem. The consistency of these measurements is examined and a mass distribution function is found which gives a best fit to the measurements. Predictions of penetration frequency are made independently of any mass determination which avoids this source of uncertainty.

The method employed is a differential technique that makes use of two or more similar observations with different thresholds to obtain values for the logarithmic derivative d log N/d log m, where N is the number of encounters per unit area-time solid angle of meteoroids with mass equal to or greater than mass m. Since it is only necessary to determine a ratio of masses characteristic to different thresholds of a given measurement technique, any multiplicative factors relating mass to the observed quantity are cancelled. A differential equation derived from the measured log derivatives gives a relation of log m and log N to within a single constant. This constant is determined to give a best fit of the resulting values estimated from each measurement. A similar differential equation is solved to give a relation between log N and log of penetration to within a single constant which is determined from an appropriate penetration measurement.

The mass distribution function was obtained from the cumulative mass flux and is found to agree remarkably well with the interplanetary dust distribution derived by Van de Hulst from interpretation of photometric measurements of F-corona and zodiacal light. It was found that interplanetary measurements of dust by Alexander on Mariner IV were in order of magnitude agreement. These results suggest that the environment is not substantially different in interplanetary space. Also, the fact that the slopes determined from satellite penetration data

appear to rapidly approach zero as N increases, suggests an upper limit on number of meteoroid encounters which appear to be on the order of $3/m^2$ day regardless of size. This low value for the maximum encounter frequency demands that a meaningful meteoroid experiment must expose an area on the order of a m^2 to collect a good statistical sample in a reasonable time.

The frequency of penetrations predicted from the analysis is much smaller for very thin material (< 0.0025-cm Al) than any previous estimate. However, the number of penetrations predicted for materials > 0.04-cm Al is more nearly approximated by the more pessimistic previous estimates. There is little doubt that the meteoroid hazard is indeed significant for vehicles with large exposures (area-time product) and that considerable emphasis must be placed on meteoroid protection in the design of such vehicles.

INTRODUCTION AND APPROACH

A detailed study of the meteoroid environment has been completed utilizing observational data taken from Explorer XVI, Explorer XXIII, Pegasus I, II, and III, as well as from radar, and photographic techniques. These observations cover the entire spectrum of masses important to the meteoroid hazard problem. The consistency of these measurements is examined and a mass distribution function is found which gives a best fit to the measurements. Predictions of penetration frequency are made independently of any mass determination which avoids this source of uncertainty.

The usual approach for obtaining a meteoroid hazard model first attempts to obtain a mass flux relation by interpreting various observations in terms of mass. Since there is no direct means for measuring mass of a meteoroid, such information must be inferred from observables such as penetration in known material, electron trail density, or emission of light. Such observables are also strongly dependent on velocity and other parameters which are not accurately known. The overall uncertainty in mass determination is estimated to be about an order of magnitude. The problem is then compounded by applying one of several empirical penetration formulas to the mass distribution to obtain a depth of penetration in a particular material.

The present approach makes a more direct use of the observational data and does not require specification of mass for any observation, thus avoiding the

major source of uncertainty. It is necessary only to know the exponent of mass in the equations relating mass to the observed quantities. There is some theoretical justification for the values of these exponents, although in some cases empirical values have been found that differ slightly from the theoretical values. The method employed is a differential technique that makes use of two or more similar observations with different thresholds to obtain values for the logarithmic derivative d log N/d log m. It is important to distinguish between the observed number of incidents per unit area-time with mass, velocity, density, etc., such that the observed quantity is above the threshold of observation, and the number N incident per unit area-time-solid angle with mass equal to or greater than some characteristic value. These quantities are related by a factor which is a function of d log N/d log m and contains integrations over angular, velocity, and density distributions. Fortunately, since present knowledge of such distributions is at best sketchy, they only enter in these correction terms, and therefore exert only a minor influence on the final result.

Since it is desirable to avoid the necessity of determining mass for any observation, the logarithmic derivatives are specified at values of log N, which are taken as the mean of the logarithms of the fluxes that determine a particular log derivative. In this manner, a set of values for the log derivative and log N are found from the observations from which a functional relation F (log N) may be found by the method of least squares. The resulting differential equation

$$\frac{d\ (\log N)}{d\ (\log m)} = F\ (\log N) \tag{1}$$

may be integrated to give

$$\log m = \int \frac{d\ \log N}{F\ (\log N)} + \text{const.} \tag{2}$$

By the previous assumption that the observable, in this case penetration of a thickness p of some specified material, is related to mass by

$$\log p = K + \gamma \log m \tag{3}$$

where K is an undetermined constant containing velocity, density, and material property terms and γ is the known exponent of mass in the equation relating mass to the observable. Therefore,

$$\log p = \gamma \int \frac{d\ \log N}{F\ (\log N)} + \text{const.} \tag{4}$$

Assuming the velocity and density distributions are independent of mass, which appears to be at least approximately the case, the above equation holds over the range for which F (log N) is known. The constant of integration which contains all the uncertainties in the definition of mass, velocity, density, and material properties may be determined by a single experiment which yields a value of N for known p of a given material. The 0.4-mm Pegasus datum point is used to obtain this constant and the derived frequency of penetration versus thickness of material applies to 2024-T3 Al backed by a soft foam.

The mass distribution function is found from the cumulative encounter frequency N. The differential equation derived from the measured log derivatives gives a relation of log m and log N to within a single constant. This constant is determined to give a best fit of the resulting values estimated from each measurement. This obviously does require the assumption of velocity and density distributions, and is also subject to errors in mass determination. However, since all the measurements are combined to find only one constant, hopefully some of these errors are averaged out, and the result is a mass distribution that is most consistent with the entire data set.

FUNDAMENTAL RELATIONS

Unfortunately, none of the present measurement techniques directly measure meteoroid mass. All such measurements have an observed quantity Q that is related to mass by an observational equation of the form

$$\log Q = \log K + \alpha \log \rho + \beta \log \mathbf{v} + \gamma \log \mathbf{m} + \delta \log \cos \theta \qquad (5)$$

where K is a constant, ρ the meteoroid density, v the meteoroid velocity, m the mass, and θ the angle of incidence. For penetration experiments, Q is the thickness of the detector; for radar observations, Q is the electron trail density; and for photographic meteors, Q is the intensity or the photographic magnitude.

Because of the spectrum of velocities, densities, and angles of incidence, there is no unique value of m corresponding to Q. The observed frequency for a given threshold Q is

$$\phi = \int_{2\pi} \int d\Omega \int_0^\infty d\rho \int_0^\infty dv \int_{m(Q,\, \rho,\, v,\, \theta)}^\infty dm \quad \cos\theta \; n_\rho(\rho) \; n_v(v) \; n_m(m) \qquad (6)$$

where $n_{\rho}(\rho)$ is the normalized density probability density function,

$n_{v}(v)$ is the normalized velocity probability density function,

$n_{m}(m)$ is the average isotropic directional mass flux differential distribution function, and $m(Q, \rho, v, \theta)$ is the threshold mass having density ρ, velocity v, and incident angle θ capable of producing Q. It is assumed that functions $n_{\rho}(\rho)$, $n_{v}(v)$, and $n_{m}(m)$ are independent.

Thus, each observation may be written as an integral equation, the set of which may be solved for the mass distribution $n_{m}(m)$.

It is useful to define a characteristic mass m_{c} of a meteoroid having normal incidence, average velocity $\langle v \rangle$ and average density $\langle \rho \rangle$ that is capable of producing a threshold Q. Obviously this m_{c} is contained in the interval of m that are the major contributors to ϕ. Further, it may be assumed that this interval is small compared to the total range of m, primarily because the mass distribution decreases rapidly for larger masses, and the velocity and density distributions decrease rapidly at some upper bound preventing the larger population of smaller masses from being observed. The intergral may be written in terms of N_{m}, the number of meteoroids with mass m or greater incident per unit area-time-solid angle,

$$N_{m} = \int_{m}^{\infty} n_{m}(m)\, dm . \tag{7}$$

Expanding $\log N_{m}$ in a Taylor's Series about $\log m_{c}$,

$$\log N_{m} = \log N_{m_{c}} + \left(\frac{d \log N_{m}}{d \log m}\right)_{m_{c}} \left[\log m - \log m_{c}\right] + \ldots \tag{8}$$

Let

$$\lambda = -\left(\frac{d \log N_{m}}{d \log m}\right)_{m_{c}} . \tag{9}$$

The minus sign is introduced for convenience so that λ will be a positive quantity.

Then

$$\int_{m}^{\infty} n_m(m)\, dm \doteq \left(\frac{m_c}{m}\right)^{\lambda} N_{m_c} \quad . \tag{10}$$

The observed flux ϕ may be written in terms of N_{m_c} the incidence flux per unit solid angle of mass m_c or greater

$$\phi = \frac{N_{m_c}}{\langle\rho\rangle^{\alpha\lambda/\gamma}\,\langle v\rangle^{\beta\lambda/\gamma}} \iint_{\text{hemisphere}} \cos^{1+\delta\lambda/\gamma}\theta\, d\Omega \int_0^{\infty} n_\rho(\rho)\rho^{\alpha\lambda/\gamma}\, d\rho \int_0^{\infty} n_v(v)\, v^{\beta\lambda/\gamma}\, dv \quad . \tag{11}$$

Integrating,

$$\phi = N_{m_c} \frac{\pi}{(1+\delta\lambda/2\gamma)} \frac{\langle \rho^{\alpha\lambda/\gamma} \rangle}{\langle\rho\rangle^{\alpha\lambda/\gamma}} \frac{\langle v^{\beta\lambda/\gamma} \rangle}{\langle v\rangle^{\beta\lambda/\gamma}} \tag{12}$$

where m_c, from its definition, is

$$\log m_c = \frac{1}{\gamma} \left(\log Q - \log K - \alpha \log\langle\rho\rangle - \beta \log \langle v\rangle\right) . \tag{13}$$

The factors appearing in the relation between incident flux and observed flux may be combined into a correction term

$$F(\lambda) = \frac{\pi}{(1+\delta\lambda/2\gamma)} \frac{\langle \rho^{\alpha\lambda/\gamma} \rangle}{\langle\rho\rangle^{\alpha\lambda/\gamma}} \frac{\langle v^{\beta\lambda/\gamma} \rangle}{\langle v\rangle^{\beta\lambda/\gamma}} \quad . \tag{14}$$

The first factor is an obliqueness correction which accounts for angles of incidence other than normal. The density and velocity terms adjust the observations according to the contributions from masses above and below the characteristic mass m_c.

Finally, the number incident having mass m_c or greater may be obtained from the observed flux by

$$N_m = \phi / F(\lambda) . \tag{15}$$

The quantity λ must be found from the log derivative

$$\lambda = - \frac{d \log N_m}{d \log m} = - \frac{d \log \phi}{d \log m} + \frac{d \log F(\lambda)}{d \log m} . \tag{16}$$

This may be solved by the method of successive approximations using as a first approximation

$$\lambda^0 = - \frac{d \log \phi}{d \log m} \doteq - \frac{\Delta \log \phi}{\Delta \log m} = -\gamma \frac{\log (\phi_1/\phi_2)}{\log (Q_1/Q_2)} \tag{17}$$

where ϕ_1 and ϕ_2 are measured rates which correspond to observables Q_1 and Q_2 for which the same observational equation applies, and γ is the mass exponent in the observational equation.

DENSITY AND VELOCITY DISTRIBUTION

The determination of a velocity distribution for meteors has been problematic because of the strong dependence of the observable on velocity. This results in a distortion of the observed velocity distribution because of the contribution of the more numerous smaller meteors on the high velocity end of the spectrum. One method of eliminating this selection effect was proposed by Orrok in which observations are categorized into groups of constant mass determined from

$$m = \frac{2}{\tau_0 v^3} \int_0^T I \, dt \tag{18}$$

where τ_0 is the luminous efficiency, T is the lifetime, and I the measured intensity. Taking a group having sufficient mass to insure practically all of the slower meteoroids will be observed should give a reasonably unbiased set of data from which a velocity distribution can be obtained.

Dohnanyi [1] applied this technique to a group of meteor observations by McCroskey and Posen and obtains a distribution function expressed by

$$n_v(v) = \begin{cases} C\, v^{1.6} & , \quad 11.2 \leq v \leq 16.6 \text{ km/sec} \\ C \times 1.61 \times 10^7\, v^{-4.3} & , \quad 16.6 < v < 72.2 \text{ km/sec} \end{cases} \tag{19}$$

where C is the normalization constant. This distribution results in $\langle v \rangle = 19.17$ km/sec. Figure 1 shows this representation.

For lack of more definitive data or contradictory evidence this distribution will be assumed to apply to the entire mass spectrum of meteors.

The density distribution is more difficult to determine. Generally, the most definitive data available is the average density of a group of observations. Jacchia, Verniani and Briggs [2] find an average ρ of 0.26 gm/cm^3 for photographic meteors. Verniani and Hawkins [3] for smaller masses find relative abundances between several groups of densities. Their tentative findings are 51 percent in a group less than 1 gm/cm^3, with an average of 0.37 gm/cm^3, 45 percent between 1 gm/cm^3, with an average of 2.8 gm/cm^3, and 4 percent greater than 12 gm/cm^3. The latter densities are of course unrealistically high, and probably result from small inaccuracies in the observed decelerations. For the lack of more definitive data, the assumed density distribution will be taken as

$$\begin{aligned} n_\rho(\rho) &= 0.51 \times 0.37\, \delta(\rho - 0.37) + 0.45 \times 2.8\, \delta(\rho - 2.8) \\ &+ 0.04 \times 8\, \delta(\rho - 8) \end{aligned} \tag{20}$$

where $\delta(\rho - \rho_1)$ are Dirac-Delta functions. The value of 8 was arbitrarily assigned to the high density component reported by Verniani which represents the highest density which could be reasonably expected. Since the observables dealt with are fairly insensitive to density and density distribution, the inaccuracies in this distribution do not significantly affect the results. This choice of distribution gives $\langle \rho \rangle = 1.77$ gm/cm^3 which is somewhat higher than usually

assumed. This is due to the higher density contributions which may indeed be significant for the smaller particles. Figure 2 shows the assumed distribution.

OBSERVATIONAL DATA

Satellite Penetration Measurements

For determining the characteristic mass for penetration of a given detector, the empirical Manned Space Center penetration formula has been utilized. This formula is usually written for semi-infinite targets in the nondimensional form

$$\frac{p}{d} = 1.64\, d^{1/18}(\text{cm})\ (\rho_p/\rho_T)^{1/2}\ (v\cos\theta/c)^{2/3} \qquad (21)$$

where p is depth of penetration

d is equivalent projectile diameter

ρ_p is projectile density

ρ_T is target density

v is projectile velocity

c is target sound velocity

θ is the angle of incidence

The constant 1.64 applies to relatively hard (2024-T3) aluminum. It is more convenient to express this formula for aluminum in the form

$$p(\text{cm}) = 0.41\, m^{0.352}\ (\text{gm})\ \rho^{0.147}\ (\text{gm/cm}^3)\ v^{0.667} \qquad (22)$$

$$(\text{km/sec})\ \cos^{2/3}\Theta.$$

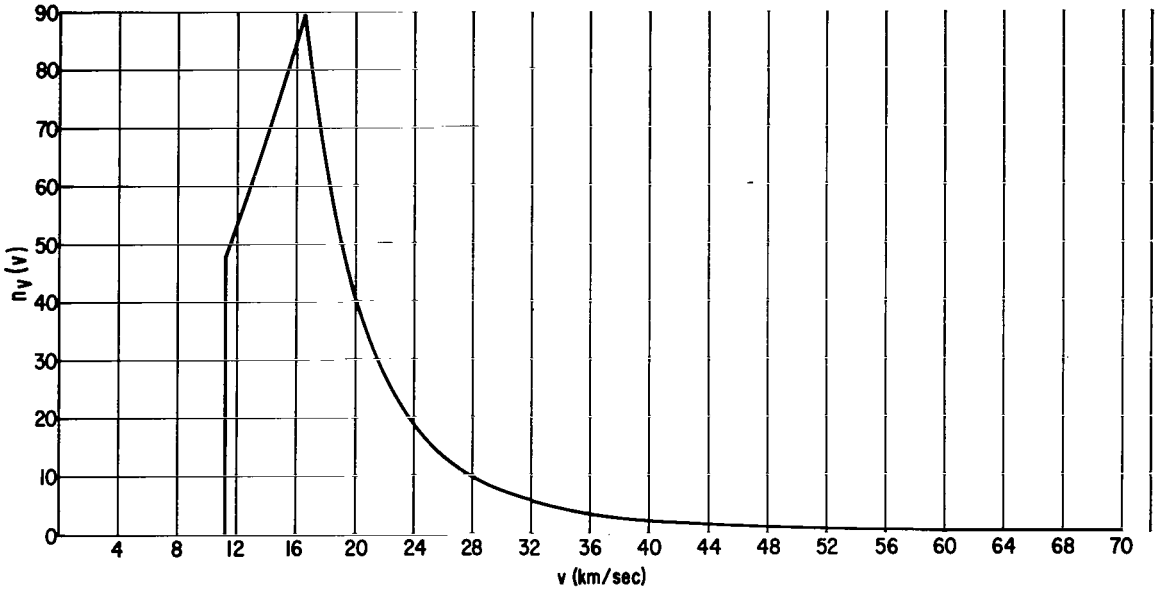

FIGURE 1. THE VELOCITY PROBABILITY DENSITY FUNCTION OBTAINED BY DOHNANYI

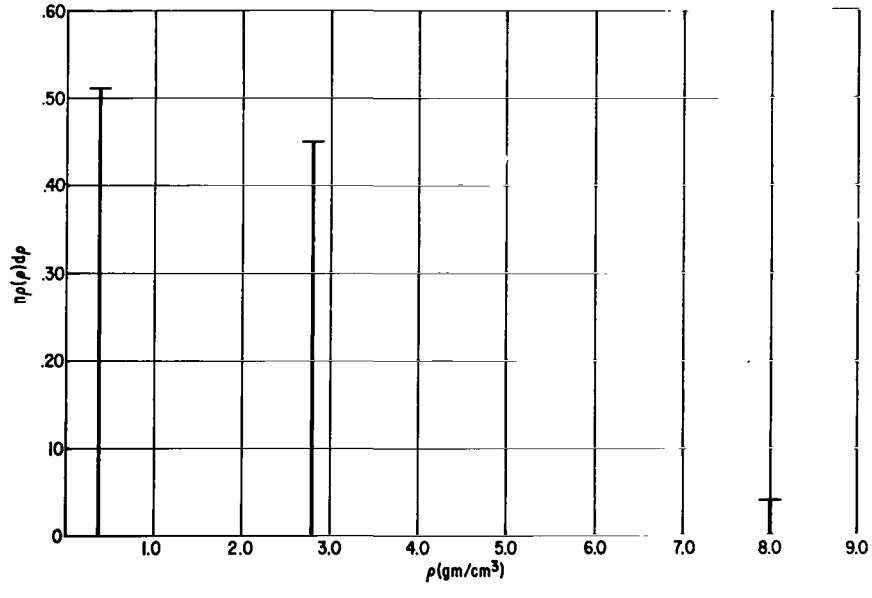

FIGURE 2. THE RELATIVE ABUNDANCES ASSUMED FOR THE VARIOUS REPRESENTATIVE DENSITIES

To correct for finite target thickness, the constant 0.41 is increased by a factor of 1.5. Thus the penetration formula may be put in the specified form for the observational equation by assigning

Q = depth of penetration (cm)

K = 0.605 for 2024-T3 Al

α = 0.147

β = 0.667

γ = 0.352

δ = 0.667

For the Cu-Be and stainless steel pressure cells used on Explorer XVI and Explorer XXIII, a factor of 2 was used to correct for finite thickness because the material is under hoop stress, has no backing, and requires only a leak for detection. Laboratory tests at AEDC [4] in stainless steel indicate a factor of 1.47 less penetration in stainless steel than in Al for velocities up to 8 km/sec. Calculations by Bjork [5] indicated a similar value for velocities of 20 and 72 km/sec. Tests at Langley Research Center indicate a similar response in Cu-Be and stainless steel at velocities up to 6 km/sec. Therefore, K is taken as $0.41 \times 2/1.47 = 0.558$ for both Cu-Be and Stainless Steel pressure cells.

Explorer XVI. - During the useful life of Explorer XVI, 44 punctures were observed in the 0.0025-cm Cu-Be pressure cells and 11 events in the 0.0050-cm cells. The rates are $0.333/m^2$ day and $0.172/m^2$ day, respectively [6]. The semimajor axis is 965 km, which results in an earth shielding factor of 0.748. The unshielded puncture rates are $0.445/m^2$ day and $0.230/m^2$ day, respectively.

From these data:

$$\lambda^0 = -\gamma \frac{\log (\phi_1/\phi_2)}{\log (Q_1/Q_2)} = 0.334 \pm 0.15$$

$$\overline{\phi} = \sqrt{\phi_1 \phi_2} = 10^{-0.495}$$

$$F(\lambda^0) = 2.21$$

$$\overline{N} = \overline{\phi}/F(\lambda^0) = 10^{-0.839}$$

Explorer XXIII. - In one year Explorer XXIII observed 49 punctures of the 0.0025-cm stainless steel pressure cells and 74 punctures in the 0.0050-cm cells. The rates are 0.345/m^2 day and 0.205/m^2 day, respectively [7]. The semimajor axis of the orbit is 390 km, which results in an earth shielding factor of 0.674. Removing this results in puncture rates of 0.526/m^2 day and 0.305/m^2 day.

From these data:

$$\lambda_0 = 0.278 \pm 0.11$$

$$\overline{\phi} = 10^{-0.397}$$

$$F(\lambda^0) = 2.32$$

$$\overline{N} = 10^{-0.763}$$

Pegasus. - Since the three Pegasus satellites had similar orbits, their data were combined. As of January 1, 1966, the 0.0038-cm detectors had counted 582 events for a rate of 0.188/m^2 day; the 0.02-cm detectors had counted 49 events for a rate of 0.021/m^2 day; and the 0.04-cm detectors had counted 201 events for a rate of 0.00487/m^2 day.[1] The shielding factor is 0.69. The unshielded rates are 0.273, 0.0305, and 0.00706/m^2 day, respectively. The aluminum thicknesses quoted are front sheets of parallel plate capacitors which are temporarily shorted by meteoroid penetration. In addition, a 0.0012-cm mylar dielectric must also be penetrated. The effect of this mylar in terms of equivalent thickness of Al is not yet known, but since it is thin compared with the 0.02 and 0.04 plate, no correction is applied to these thicknesses. The mylar is a significant fraction of the 0.0038-cm detector and must be considered in this case. Also, the 0.0038-cm detector is 1100-0 aluminum rather than 2024-T3, and is backed with a 0.013-cm hard epoxy layer rather than soft foam. An effective thickness in terms of the 0.02- and 0.04-cm detectors has not yet been accurately determined; therefore, this datum point will not be used to determine the slope of the penetration curve. From the 0.02-cm and 0.04-cm points,

$$\lambda^0 = 0.740 \pm 0.14$$

$$\overline{\phi} = 10^{-1.841}$$

---

1. Clifton, K.S. and Naumann, R.J.: Pegasus Satellite Measurement of Meteoroid Penetration. NASA TM X (in publication).

$F(\lambda^0) = 1.76$

$\overline{N} = 10^{-2.076}$

Radar Observations

Elford [8] using a transmitted power of 1.2 megawatts, reported a total flux of $9.05 \times 10^{-4}/m^2$ day of meteors whose maximum line densities exceed 3.3×10^{10} e/m. Reducing the transmitted power by a factor of 143 resulted in a decrease in observed echoes by a factor of 12. Assuming the reflected electric field vector is proportional to the average trail density, the transmitted power required for a given reflected power varies as the inverse square of the electron line density. Thus, the minimum detectable line density for the low power operation is 3.94×10^{11} e/m.

Using the ionization efficiency determined by Verniani [9], the maximum line density (e/m) may be related to mass by

$$\log q = 10.638 + \log m + 4 \log v + \cos \theta \qquad (23)$$

where v is in km/sec and m is in grams.

The observational equation may be specified by setting

Q = electron line density, q (e/m)

$\log k = 10.638$

$\alpha = 0$

$\beta = 4$

$\gamma = 1$

$\delta = 1$

The earth shielding factor is unity since the area in question is parallel to and facing away from the earth.

The first approximations are

$\lambda^0 = 1.005 \pm ?$

$\overline{\phi} = 10^{-3.583}$

$F(\lambda^0) = 5.94$

$\overline{N} = 10^{-4.358}$

Photographic Observations

Hawkins and Upton [10] determined the influx rate of photographic meteors in the range of -2.5 to +3 photographic magnitude. Their observed flux may be expressed in terms of peak photographic magnitude Mp or brighter as

$$\log \phi = 0.537\ Mp - 8.95\ (no./m^2\ day). \tag{24}$$

The uncertainty in this relation is least from $-2.0 \leq Mp \leq 2.5$.

Jacchia, Verniani, and Briggs [3] performed a detailed analysis of a selected group of Super-Schmidt meteors whose masses were determined by integration of the total light curve. They found by method of least-squares a relation for peak brightness given by

$$Mp = 11.59 - 8.75 \log v - 2.25 \log m - 1.5 \log \theta\ . \tag{25}$$

$\log Q = Mp$

$\log K = 11.59$

$\alpha = 0$

$\beta = -8.75$

$\gamma = -2.25$

$\delta = -1.5$

From these data

$$\lambda^0 = 1.205 \pm 0.06$$

$$\overline{\phi} = 10^{-8.815}$$

$$F(\lambda^0) = 10.41$$

$$\overline{N} = 10^{-9.832}$$

COMPUTATION PROCEDURE

The correction factor $F(\lambda)$ which relates observed number to cumulative directional flux depends on the measurement involved. This factor is shown in Figure 3 for penetration, radar, and photographic measurements. A few comments concerning the interpretation of this factor may be in order. The factor contains π which, when multiplied by the number per steradian, gives the total number incident on a flat surface. For penetration observations, the fact that $F(\lambda)$ is less than π means that most of the observed punctures are caused by meteoroids with mass greater than the characteristic mass. This is primarily because of the reduced penetrating ability of particles impacting obliquely. For the radar and photographic observations, the large velocity dependence allows a significant number of the more numerous meteors with masses smaller than m_c but with velocities higher than average to be observed; hence, the value of $F(\lambda)$ is greater than π.

The first approximations for λ versus $y = -\log N$ are shown in Figure 4. Successive approximations may be obtained by the following process. Taking the log of equation (15) and differentiating,

$$d \log N = d \log \phi - \frac{d \log F(\lambda)}{d\lambda} \frac{d\lambda}{d \log N} d \log N \qquad (26)$$

Let $x = \log m$, $y = -\log N$

$$\frac{dy}{dx} = -\frac{d \log \phi}{dx} + \frac{d \log F(\lambda)}{d\lambda} \frac{d\lambda}{dy} \frac{dy}{dx} \qquad (27)$$

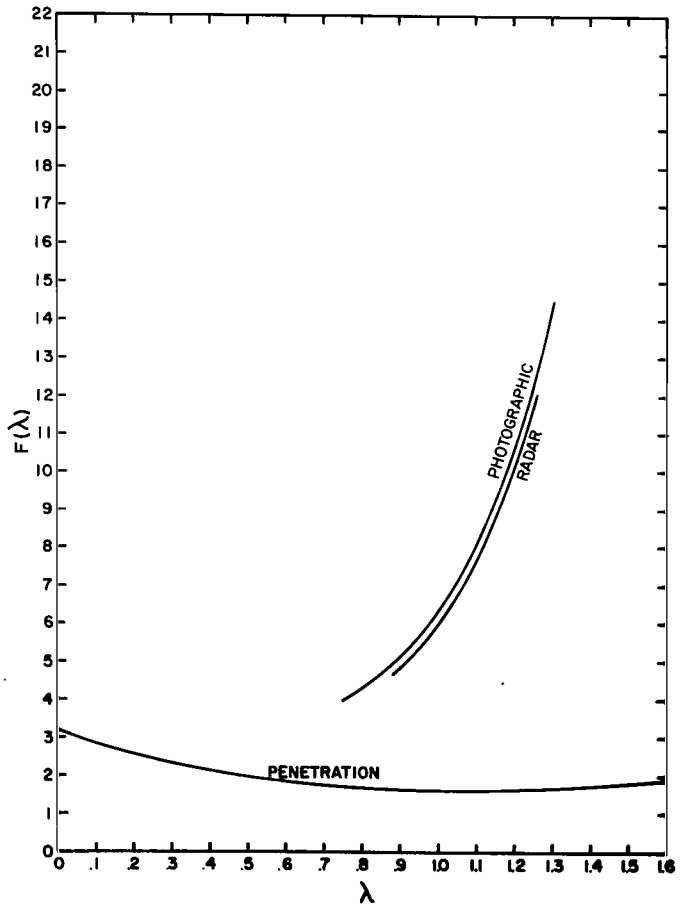

FIGURE 3. THE RATIO F(λ) OF THE OBSERVED FLUX OF METEOROIDS TO THE NUMBER ENCOUNTERED PER UNIT AREA TIME-SOLID-ANGLE WITH MASS SUFFICIENT TO PRODUCE A THRESHOLD OBSERVATION PROVIDED THEY HAVE AVERAGE DENSITY, AVERAGE VELOCITY, AND NORMAL INCIDENCE

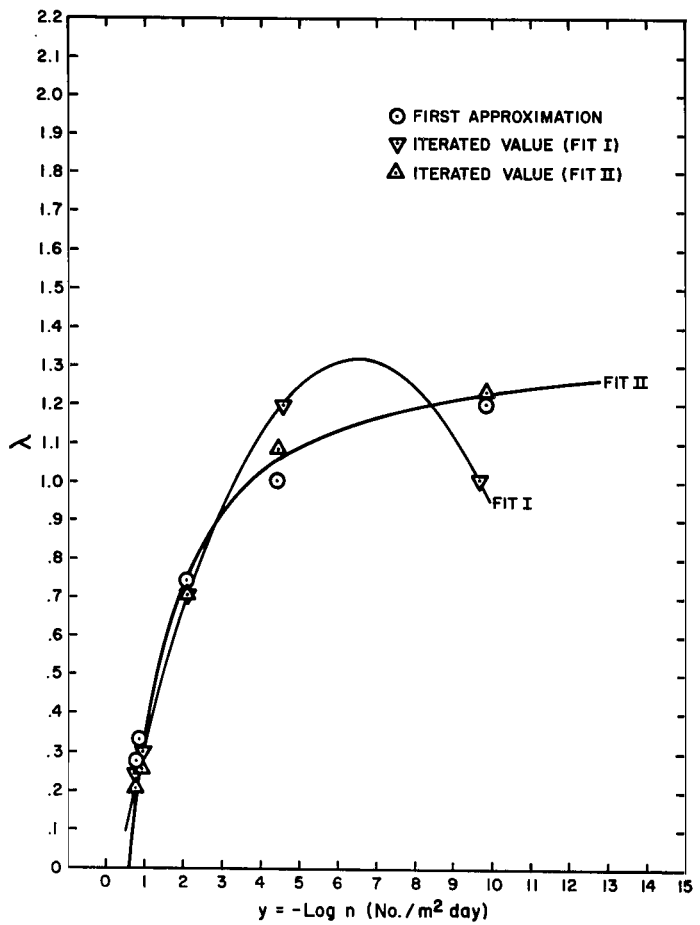

FIGURE 4. THE POSSIBLE FITS TO λ AS A FUNCTION OF Y. THE DEPARTURES OF THE ITERATED VALUES OF FIT I FROM THE OBSERVED VALUES ARISE FROM THE CORRECTIONS IN λ INVOLVING dλ/dy

By definition,

$$\lambda = \frac{dy}{dx} \; ; \quad \lambda^0 = -\frac{d \log \phi}{dx} \quad \therefore \quad \lambda = \lambda^0 / \left[1 - \frac{d \log F(\lambda)}{d\lambda} \frac{d\lambda}{dy} \right] . \tag{28}$$

A functional relation for $\lambda^i = \lambda(y^i)$ is found by the method of least squares and is used to compute $d\lambda^i/dy^i$. The $(i + 1)^{th}$ approximation is found for each measurement from

$$\lambda^{i+1} = \lambda^0 / \left[1 - \frac{d \log F(\lambda^i)}{d\lambda^i} \frac{d\lambda^i}{dy^i} \right] \tag{29}$$

The $(i + 1)^{th}$ approximation for each y is then found from

$$y^{i+1} = \log F(\lambda^{i+1}) - \log \overline{\phi} \tag{30}$$

The process continues until $\lambda^{i+1} = \lambda^i$ for each value of λ.

The question of the analytical representation for $\lambda = \lambda(y)$ must be considered. The most straightforward choice that could provide a reasonable fit is a second degree polynominal,

$$\lambda = ay^2 + by + c \tag{31}$$

It may be seen from Figure 3 that $d \log F(\lambda)/d\lambda$ is negative for penetration observations for $\lambda < 1.1$, and that it is positive for radar and photographic observations in the range of λ applicable. Since the first approximations for λ in Figure 4 indicate positive but decreasing value of $d\lambda/dy$ for increasing y, it may be seen from equation (28) that the values of λ for penetration observations will be decreased while those corresponding to radar and photographic observations increase. Because of the larger $d\lambda/dy$ at the radar point, the corresponding λ is increased more than the λ corresponding to the photographic point. This causes the polynomial fit to reach a maximum before the photographic point and $d\lambda/dy$ becomes negative at the photographic point. This change of sign forces the corrected λ for the photographic point to have a smaller value, and the final result is that indicated by Fit I in Figure 4. Physically, this may be interpreted to mean that the mass distribution is such that the higher velocity tail of the velocity distribution, which allows the more numerous smaller mass meteors to be above the observational threshold, is less effective for the larger masses than for the smaller masses. Hence the observed slope $d \log \phi / d \log m$ is steeper than the true slope $d \log N / d \log m$.

There is, of course, no theoretical justification in the choice of the polynomial chosen to represent $\lambda(y)$. The peak in λ between the radar and photographic data may not correspond to physical reality. For this reason, an alternative representation was chosen that conditions $\lambda(y)$ to be monotonic, i.e.,

$$\frac{1}{\lambda} = a + \frac{b}{y - c} \tag{32}$$

The results of this choice are indicated as Fit I in Figure 4. There appears to be considerable difference in the two results, which more or less represent extremes in the possible choices for $\lambda(y)$. Fortunately, however, the end results, such as finding a mass distribution or penetration frequency, are not seriously influenced by the choice of representation of $\lambda(y)$.

The cumulative mass distribution may be found to within a constant of integration by solving the differential equation

$$\frac{dy}{dx} = \lambda(y) \tag{33}$$

or

$$\log m = \int \frac{dy}{\lambda(y)} + d \tag{34}$$

For Fit I,

$$\log m = \frac{-2}{\sqrt{b^2 - 4ac}} \tanh^{-1} \left[\frac{-2a \log N + b}{\sqrt{b^2 - 4ac}} \right] + d_I \tag{35}$$

where from the fit of $\lambda = \lambda^I(y)$

$$a = -0.0328156$$

$$b = 0.425222$$

$$c = -0.550693$$

For Fit II,

$$\log M = -a \log N - b \ln(-\log N - c) + d_{II} \tag{36}$$

where a, b, c have been determined from the fit of $\lambda = \lambda^{II}(y)$

$a = 0.719683$

$b = 0.858195$

$c = 0.590827$

A value for d was computed for each datum point. Table I is a summary of these results. The average value and RMS deviation in d is -2.35 ± 0.53 for Fit I and -8.45 ± 0.46 for Fit II, with the radar points producing the largest deviations in both cases. Using the average value for d, the cumulative mass distribution is shown in Figure 5. It may be seen that the satellite points fall slightly to the right of the mass distribution and photographic points fall slightly to the left. This means that meteoroids are either somewhat more penetrating than predicted from the MSC formula or that the masses inferred from photographic data are too small. The radar points fall considerably on the small side. However, the uncertainty of ± 0.3 in the velocity exponent of the radar observational equation estimated by Verniani [3] is sufficient to bring these points into agreement.

It is not necessary to actually use the mass estimates with their inherent uncertainties to obtain an expression for penetration frequency. Since penetration

$$p \sim m^{\gamma} , \tag{37}$$

$$\log p = \gamma \log m + \text{constant} \tag{38}$$

$$\log p = -1.6897 \tanh^{-1} [0.1575 \log N + 1.0206] + d^{*}_{I} \tag{39}$$

for Fit I, or for Fit II,

$$\log p = -0.2533 \log N - 0.3021 \ln (-\log N - 0.5910) + d^{*}_{II} \tag{40}$$

The constant d^{*} now contains the combination of material velocity, and density terms in the penetration formula as well as the constant of integration in the mass distribution. This constant can be determined for a particular material from a single penetration measurement. Using the Pegasus 0.04-cm datum point,

$d^{*}_{I} = -0.1054$

$d^{*}_{II} = -2.060$

TABLE Ia

Fit I

Measurement	ϕ Obs. no./m^2 day	λ	$F(\lambda)$	N no./m^2 day sterad	log d	Est. Mass (gm)	Mass From Fit (gm)
.04 cm. Peg.	$10^{-2.16}$	.773	$10^{.230}$	$10^{-2.39}$	-2.230	$10^{-5.91}$	$10^{-6.03}$
.02 cm. Peg.	$10^{-1.53}$	.601	$10^{.264}$	$10^{-1.79}$	-2.211	$10^{-6.76}$	$10^{-6.90}$
.0050 cm. Exp. XXIII	$10^{-.516}$	.292	$10^{.360}$	$10^{-.876}$	-1.673	$10^{-8.33}$	$10^{-9.01}$
.0025 cm. Exp. XXIII	$10^{-.278}$	.215	$10^{.392}$	$10^{-.670}$	-1.709	$10^{-9.19}$	$10^{-9.83}$
.0050 cm. Exp. XVI	$10^{-.638}$	.331	$10^{.345}$	$10^{-.983}$	-2.017	$10^{-8.33}$	$10^{-8.67}$
.0025 cm. Exp. XVI	$10^{-.352}$	.239	$10^{.382}$	$10^{-.734}$	-1.990	$10^{-9.19}$	$10^{-9.55}$
Low Power Radar	$10^{-4.12}$	1.270	$10^{1.092}$	$10^{-5.21}$	-3.209	$10^{-4.18}$	$10^{-3.32}$
High Power Radar	$10^{-3.04}$	1.109	$10^{.888}$	$10^{-3.93}$	-3.210	$10^{-5.25}$	$10^{-4.40}$
-2 Photo. Mag.	$10^{-10.02}$	.760	$10^{.597}$	$10^{-10.62}$	-2.686	$10^{1.05}$	$10^{1.38}$
2.5 Photo. Mag.	$10^{-7.61}$	1.176	$10^{.981}$	$10^{-8.59}$	-2.608	$10^{-.948}$	$10^{-.694}$

TABLE Ib

Fit II

Measurement	ϕ Obs. no./m^2 day	λ	$F(\lambda)$	N no./m^2 day sterad	log d	Est. Mass (gm)	Mass From Fit (gm)
.04 cm. Peg.	$10^{-2.16}$	.833	$10^{.221}$	$10^{-2.38}$	-8.116	$10^{-5.91}$	$10^{-6.24}$
.02 cm. Peg.	$10^{-1.53}$	.690	$10^{.244}$	$10^{-1.77}$	-8.175	$10^{-6.76}$	$10^{-7.03}$
.0025 cm. Exp. XXIII	$10^{-.516}$	.273	$10^{.368}$	$10^{-.884}$	-7.911	$10^{-8.33}$	$10^{-8.87}$
.0050 cm. Exp. XXIII	$10^{-.278}$	.125	$10^{.433}$	$10^{-.711}$	-7.867	$10^{-9.19}$	$10^{-9.77}$
.0025 cm. Exp. XVI	$10^{-.638}$	.341	$10^{.342}$	$10^{-.980}$	-8.224	$10^{-8.33}$	$10^{-8.55}$
.0050 cm. Exp. XVI	$10^{-.352}$	.173	$10^{.410}$	$10^{-.762}$	-8.215	$10^{-9.19}$	$10^{-9.42}$
Low Power Radar	$10^{-4.12}$	1.09	$10^{.869}$	$10^{-4.99}$	-9.042	$10^{-4.18}$	$10^{-3.58}$
High Power Radar	$10^{-3.04}$	1.02	$10^{.785}$	$10^{-3.83}$	-9.014	$10^{-5.25}$	$10^{-4.68}$
-2 Photo. Mag.	$10^{-10.02}$	1.25	$10^{1.07}$	$10^{-11.09}$	-8.948	$10^{1.05}$	$10^{1.55}$
2.5 Photo. Mag.	$10^{-7.61}$	1.21	$10^{1.02}$	$10^{-8.63}$	-8.950	$10^{-.948}$	$10^{-.44}$

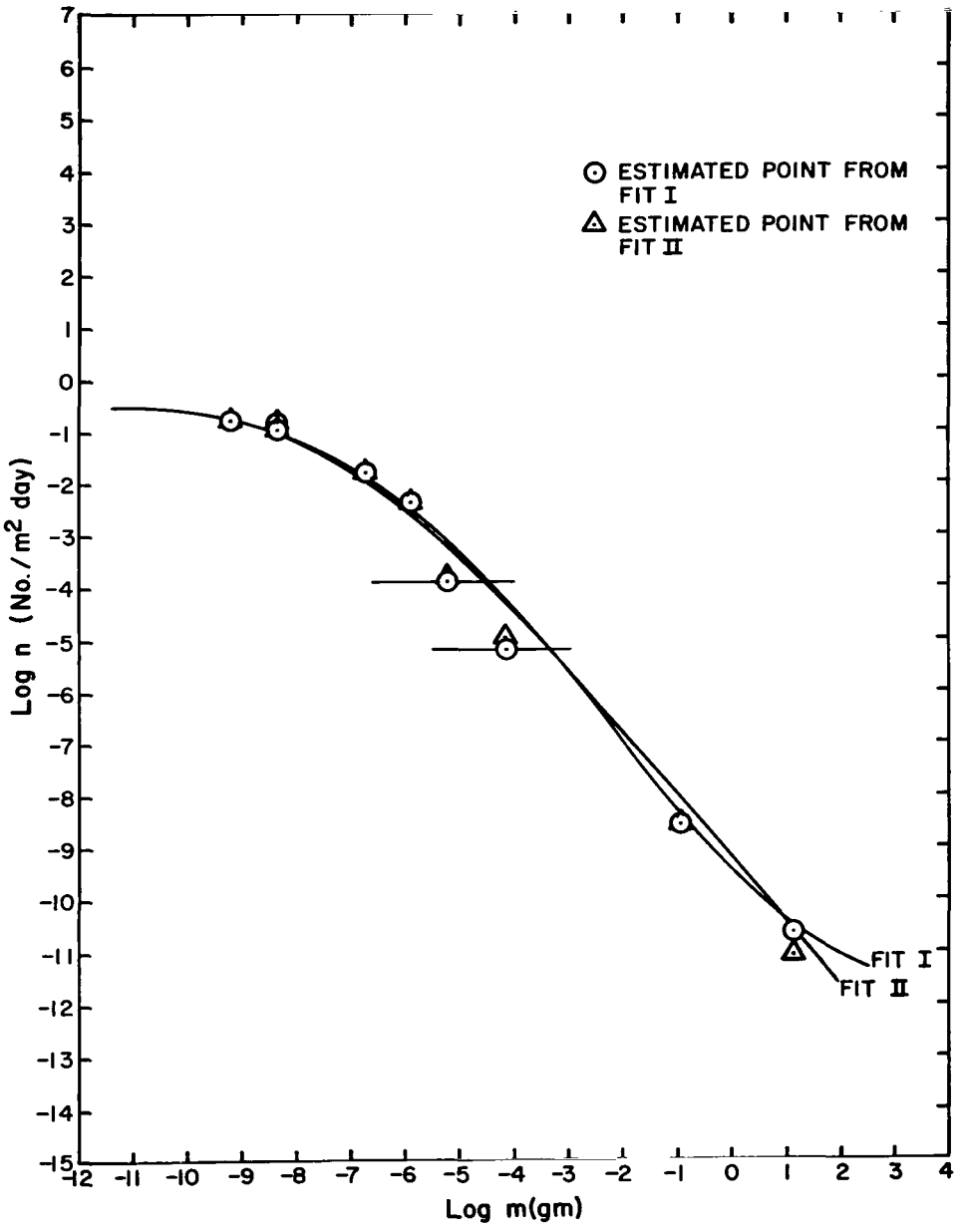

FIGURE 5. THE CUMULATIVE MASS FLUX DISTRIBUTION THAT BEST FITS THE ESTIMATED CHARACTERISTIC MASS FOR EACH MEASUREMENT. THE ERROR BARS ON THE RADAR POINTS IN THE VICINITY OF 10^{-5} gm INDICATE THE RESULT OF UNCERTAINTY OF THE DEPENDENCE OF IONIZATION EFFICIENCY ON VELOCITY

PENETRATION FREQUENCY

Figure 6 is a plot of the estimated frequency of penetration versus thickness of 2024-T3 Al backed with foam. These same curves may be used for any other material by establishing an equivalent thickness of 2024-T3 for the material by laboratory impact tests. The pessimistic curve results from Fit II. The maximum difference between Fit I and II is a factor of 0.4-in. thickness required to give a certain penetration frequency. It is recommended that the largest value be used in all cases for a conservative design value. Table II is a summary of penetration frequency for various thickness of 2024-T3 Al.

The other possible source of uncertainty in the penetration formula lies in the values of γ used in obtaining the log derivatives. Recall that empirical values of $\gamma = 0.352$ for penetration calculations and $\gamma = -2.25$ were used for photographic analysis. These are slightly different from their respective theoretical counterparts of 0.333 and -2.5.

To investigate the possible effects of this uncertainty, the calculations were also run with these values. The optimistic curve results from Fit I with the smaller values of γ, i.e., 0.333 and -2.5. Since the two major sources of uncertainty, i.e., the choice of analytical representation and the mass exponents have been analyzed with more or less extreme cases, the envelope of the resulting penetration curves may be considered to represent the limits with which penetrating flux can be predicted with available data. Although the limits diverge with increasing thickness, the spread is only a factor of 2 in thickness for the largest thickness of interest. Other choices of velocity or density distributions have virtually no effect on this result.

For thicknesses less than 0.04 cm, the difference between the various cases is less. Figure 7 is an expanded plot of this region. The problem of material equivalence between the 0.0038-cm Pegasus point, the Explorer XVI points, and the Explorer XXIII points is avoided by the fact that the technique uses the slopes and the number observed rather than the actual thickness. Values for material equivalence can be inferred from this plot by taking the thickness in 2024-T3 Al from the plot that corresponds to the observed penetration frequency. The results are:

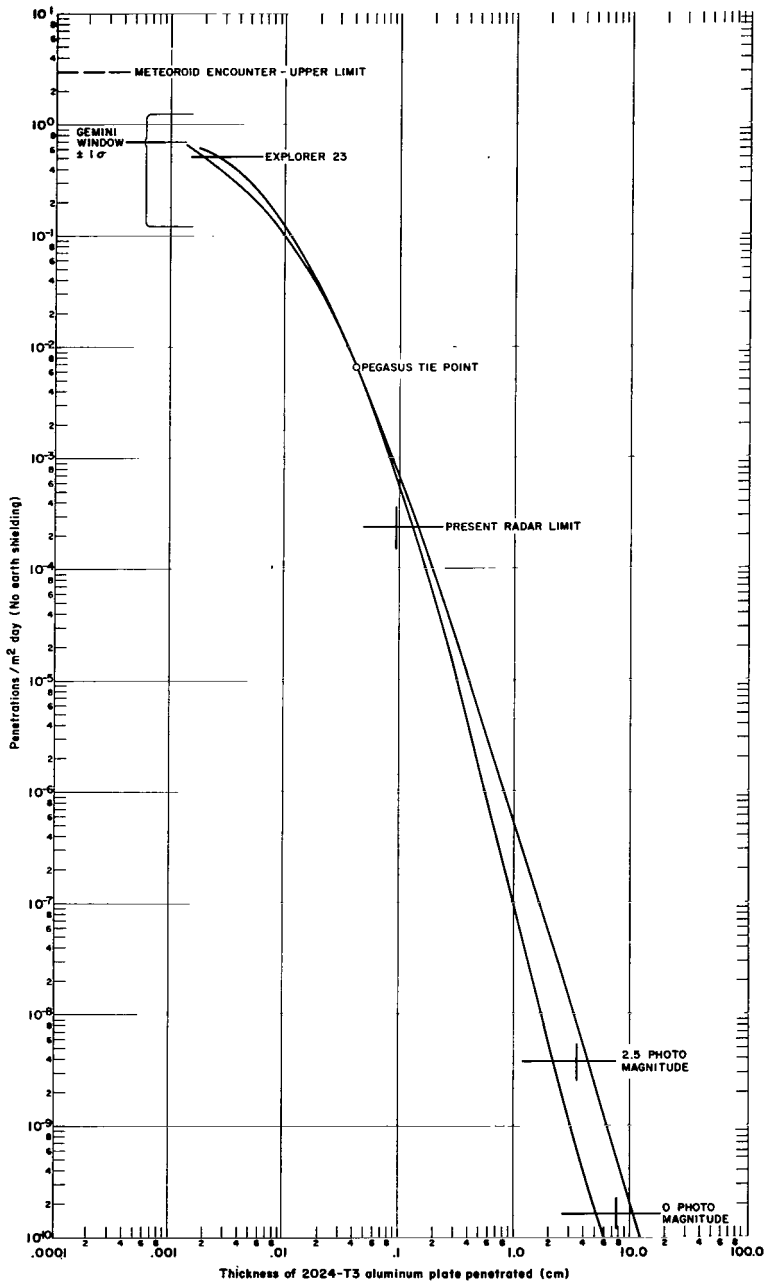

FIGURE 6. ESTIMATED PENETRATION FREQUENCY IN VARIOUS THICKNESSES OF 2024-T3 Al. THE ENVELOPE REPRESENTS LIMITS OF COMBINED UNCERTAINTIES IN MASS DEPENDENCE AND FORM OF FUNCTIONAL FITS. THE INDICATED MEASUREMENTS ARE PENETRATION RATES ESTIMATED ON THE BASIS OF THE CALCULATED CHARACTERISTIC MASS FOR EACH MEASUREMENT

TABLE II

Thickness 2024-T3 Plate (cm)	Upper Limit no./m^2 day	Lower Limit no./m^2 day
.003	4.40×10^{-1}	3.60×10^{-1}
.004	3.52×10^{-1}	2.72×10^{-1}
.005	2.81×10^{-1}	2.15×10^{-1}
.006	2.31×10^{-1}	1.70×10^{-1}
.007	1.92×10^{-1}	1.40×10^{-1}
.008	1.63×10^{-1}	1.19×10^{-1}
.009	1.49×10^{-1}	1.01×10^{-1}
.010	1.19×10^{-1}	8.90×10^{-2}
.020	3.35×10^{-2}	2.90×10^{-2}
.030	1.39×10^{-2}	1.28×10^{-2}
.040	7.10×10^{-3}	7.10×10^{-3}
.050	4.30×10^{-3}	4.30×10^{-3}
.060	2.50×10^{-3}	2.36×10^{-3}
.070	1.77×10^{-3}	1.60×10^{-3}
.080	1.28×10^{-3}	1.10×10^{-3}
.090	8.50×10^{-4}	7.40×10^{-4}
.100	6.50×10^{-4}	5.40×10^{-4}
.200	8.50×10^{-5}	5.60×10^{-5}

TABLE II (Concluded)

Thickness 2024-T3 Plate (cm)	Upper Limit no./m^2 day	Lower Limit no./m^2 day
.300	2.50×10^{-5}	1.20×10^{-5}
.400	9.50×10^{-6}	4.00×10^{-6}
.500	4.98×10^{-6}	1.65×10^{-6}
.600	2.70×10^{-6}	7.90×10^{-7}
.700	1.61×10^{-6}	4.10×10^{-7}
.800	1.09×10^{-6}	2.40×10^{-7}
.900	7.30×10^{-7}	1.46×10^{-7}
1.000	5.20×10^{-7}	9.50×10^{-8}
2.000	5.40×10^{-8}	5.80×10^{-9}
3.000	1.30×10^{-8}	1.15×10^{-9}
4.000	5.02×10^{-9}	4.00×10^{-10}
5.000	2.40×10^{-9}	1.89×10^{-10}
6.000	1.29×10^{-9}	1.10×10^{-10}
7.000	7.40×10^{-10}	6.80×10^{-11}
8.000	4.60×10^{-10}	4.50×10^{-11}
9.000	3.00×10^{-10}	3.10×10^{-11}
10.000	2.10×10^{-10}	2.30×10^{-11}

Detector Material and thickness (cm)	Equivalent thickness in 2024-T3 Al (cm)	Equivalence Factor
0.0025 Cu-Be	0.0028 ± 0.0009	1.12 ± 0.36
0.0050 Cu-Be	0.0056 ± 0.0020	1.12 ± 0.40
0.0025 Stainless	0.0021 ± 0.0009	0.84 ± 0.36
0.0050 Stainless	0.0042 ± 0.0010	0.84 ± 0.20
0.0038 1100 Al	0.0046 ± 0.0007	1.21 ± 0.18

It may be seen that all the sensors have material equivalence factors near unity, which means they are essentially equivalent to 2024-T3 Al. It is known that both stainless steel and Cu-Be semi-infinite target are penetrated less deeply by hypervelocity projectiles. However, apparently this is compensated somewhat by the fact that these detectors have a free rear surface which is more subject to spall than a foam-backed material. Recall that the estimated equivalence factor (Page 11) was 1.11, which is in good agreement with the derived value for Cu-Be. It appears that the stainless steel is not as puncture resistant as the Cu-Be since the puncture rates in both thicknesses of stainless steel exceed the corresponding rates in Cu-Be, and the slope determined from the data points is not as steep for Explorer XXIII. Of course the small statistical sample does not permit this to be stated definitely. The difference between the observed rates in the 0.0025-cm detectors is 18 percent while the standard deviations associated with the rates are approximately 14 percent. Also, the standard deviations in the slope are not sufficiently small to say that the slope corresponding to stainless steel is actually less than that of the Cu-Be. The 0.0038-cm Pegasus detector has a 0.0012-cm mylar backing that also must be penetrated to produce a signal. Thus, the total material thickness is actually 0.005 cm which is quite close to the 0.0046-cm equivalent thickness. Apparently the fact that 1100 Al has lower strength than the 2024-T3 is compensated by the thick epoxy backing on the 0.0038 cm-Pegasus detector.

MASS DISTRIBUTION

As was seen in Figure 5, the cumulative mass distribution obtained from either fit agrees with the values estimated from the various measurements to

within ± approximately half an order of magnitude. Both representations produce computed values of λ that agree with the observed values to within observational limitations.

	λ^0 OBS	λ^0 Fit I	λ^0 Fit II
Explorer XVI	0.334 ± 0.15	0.324	0.331
Explorer XXIII	0.278 ± 0.11	0.290	0.264
Pegasus	0.740 ± 0.14	0.724	0.794
Radar	1.006 ± ?	1.007	0.980
Photographic	1.205 ± 0.06	1.160	1.206

The Fit I gives slightly less difference between the constant of integration determined from the Pegasus points and that determined from the photographic points. This difference is 0.47 in the logarithim or a factor of 3 in mass. It is reasonable to assume that such a difference can be accounted for by our imperfect knowledge of penetration mechanics, particularly for threshold penetrations in finite targets, and by the uncertainty inherent in inferring mass from photographic observations.

The differential directional mass flux distribution function $n_m(m)$ can be constructed for any value of mass m_o from

$$n_m(m_o)\, dm = N_{m_o - dm} - N_{m_o} \tag{41}$$

using the Taylor expansion for N_m about m_o, equation (10),

$$n_m(m_o)\, dm = \left(\frac{m_o - dm}{m_o}\right)^{-\lambda} N_{m_o} - N_{m_o} \tag{42}$$

$$n_m(m_o) = \frac{\lambda}{m_o} N_{m_o} \tag{43}$$

The resultant mass distribution is shown in Figure 8. It is interesting to compare this derived mass distribution with that of Van de Hulst [11] obtained from interpretation of the F-component of the solar corona and zodiacal light in terms of light diffracted from dust particles in interplanetary space. Van de Hulst finds the photometric data can be well represented by a distribution in radii by

$$N(a) = c\ a^{-2.6} \quad (\text{no./cm}^3) \tag{44}$$

where

$$c = \begin{cases} 10^{-20} & \text{at 1 A. U.} \\ 3.5 \times 10^{-19} & \text{at 0.5 A. U.} \\ 0 & < 0.1 \text{ A. U.} \end{cases}$$

for $a < 0.035$ cm.

Taking the average density as 1.7 gm/cm^3 and the average velocity as 20 km/sec, this distribution can be transformed to a distribution in directional mass flux encountered by an object in an orbit similar to that of the earth,

$$n_m(m) = 1.25 \times 10^{-6}\ m^{-1.534} \quad (\text{No./m}^2 \text{ day str. gm}).$$

It may be seen from Figure 6 that the agreement both in magnitude and slope between the mass distributions is remarkable for masses from 10^{-5} gm to 10^{-10} gm. Van de Hulst states that particles with radii < 0.035 cm are less abundant than indicated by his distribution function, which agrees very well with present result.

A flattening and possible eventual decline of the distribution function for smaller masses would be expected as the result of the increased significance of radiation perturbations such as Poynting-Robertson effect and radiation pressure. The derived expressions for N approach a maximum value for the incident number which is 0.738/m^2 day steradian for Fit I and 0.255/m^2 day steradian for Fit II. The existing data do not extend to small enough masses to determine this accurately, but it is reasonably certain that only approximately 2-3 encounters/m^2 day can be expected with all meteoroids regardless of their mass. This is consistent with the fact that only one encounter in 1.4/m^2 day exposure has been observed on Gemini windows[1] which sets a 90 percent upper limit of 2.8/m^2 day on events that produce discernable damage to optical surfaces. It is

1. Burbank, P.: Manned Space Center, private communication, 1966.

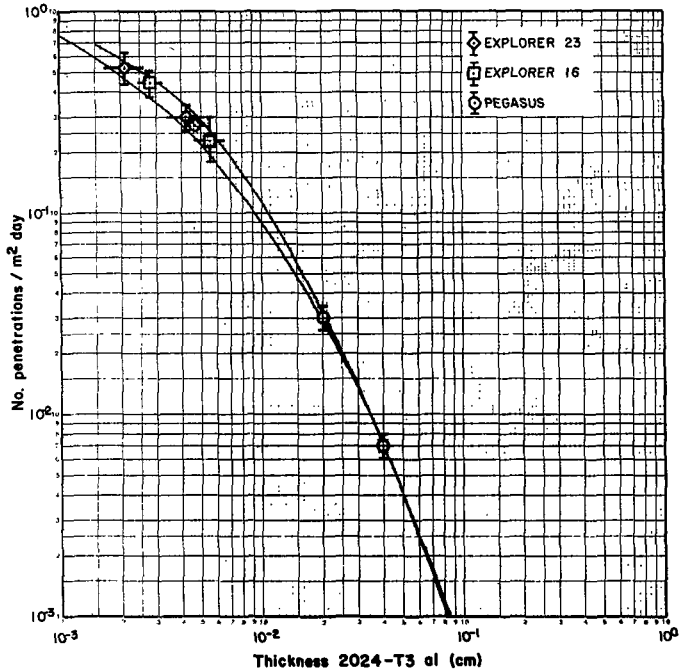

FIGURE 7. AN EXPANDED REGION OF THE PENETRATION CURVE. THE EXPLORER POINTS AND THE 0.038 mm PEGASUS POINT WERE ADJUSTED IN THICKNESS TO AGREE WITH THE SLOPE OF THE PENETRATION CURVE. THE RESULTING VALUE IS TAKEN AS THE EQUIVALENT THICKNESS IN 2024-T3 Al

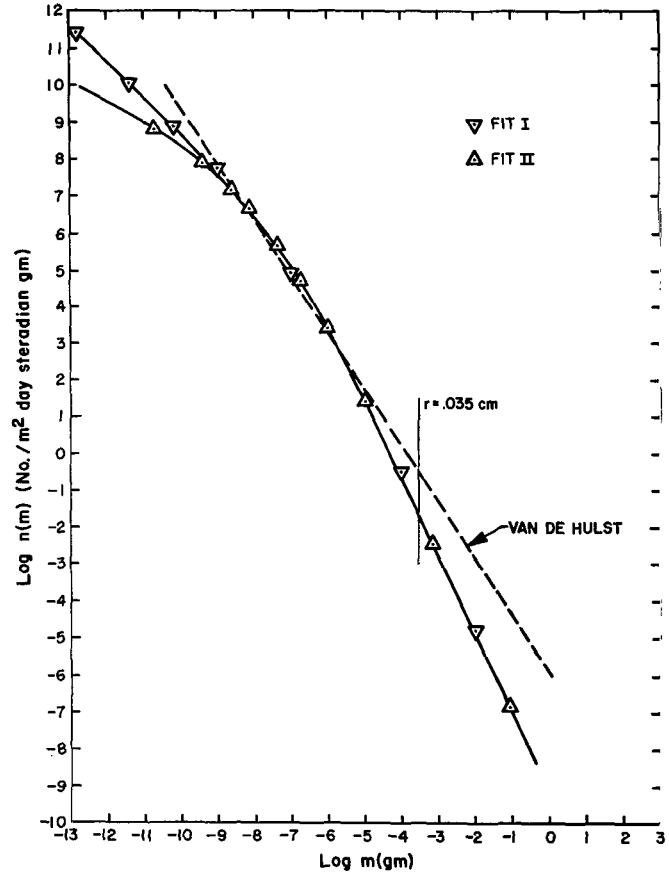

FIGURE 8. THE DIRECTIONAL MASS FLUX PROBABILITY DENSITY FUNCTION COMPARED WITH ESTIMATES OBTAINED FROM ZODIACAL LIGHT BY Van de HULST

also interesting to note that meteoroid measurements from Mariner IV [12] from 1 - 1.56 A. U. observe between 0.63 and 2.8 events/m^2 day.

No value for cut-off mass due to radiation pressure if one indeed exists[1] can be inferred from the functions derived from either Fit I or II because the mass corresponding to the maximum N is 0. The mass contribution $m\, n_m(m)\, dm$ from the particles smaller than 10^{-13} gm is negligible. The total mass influx may be found by integrating

$$m_T = \iint_{2\pi} \cos\theta \, d\Omega \int_0^\infty m\, n_m(m)\, dm \quad . \tag{45}$$

Since $n_m(m) = \dfrac{\lambda N_m}{m}$

$$m_T = \pi \int_0^\infty \lambda \; N_m \, dm \; .$$

For a small interval (m_1, m_2) the contribution in mass influx is found approximately using the Taylor expansion for N_m about m_1

$$m_{12} = \pi \int_{m_1}^{m_2} \lambda \left(\frac{m}{m_1}\right)^{-\lambda} N_{m_1} \, dm \tag{46}$$

$$m_{12} = \frac{\pi \lambda N_{m_1} m_1^{\lambda}}{1 - \lambda} \left[m_2^{1-\lambda} - m_1^{1-\lambda} \right] \quad . \tag{47}$$

The total mass influx is found by summing the incremental contributions. This presents no problem for Fit II since λ approaches an asymptotic value greater than unity. However, using Fit I, λ approaches 0 for masses greater than those corresponding to the photographic data. This leads to an infinite mass influx if the integration is carried to $m = \infty$. Since such masses exceed the limits of the data, there is no justification for extending the derived expression

---

1. Often this limit is estimated by equating gravitational force to radiation pressure applied to the geometrical cross section of a sphere and solving for the radius. This does not hold for dielectric particles or particles whose dimensions are of the order of or less than a visible wavelength. In fact Shapiro showed that submicron metallic and all sizes of SiO_2 particles never have radiation pressure forces greater than gravitational forces.

for N_m into this region. Therefore the summation is carried only to the last datum point. The mass influx contributions for larger masses are believed to be insignificant because of the rapidly decreasing population. If, for example, the value for λ for masses greater than 10 gm is 1.2, the contribution from larger masses is only 3 percent of the total.

The total mass influx is found by 2.7×10^{-7} gm/m^2 day for Fit I and 1.4×10^{-7} gm/m^2 day for Fit II. This leads to a mass accretion of around 100 metric tons per day. This is considerably less than earlier estimates based on extrapolation of photographic meteors to smaller masses which ranged from 1000 to 10 000 tons per day.

Having determined the mass distribution, there are several other quantities of interest that may be easily found. The normal component of momentum flux may be found from

$$mv_\perp = \iint_{2\pi} d\Omega \cos\theta \int_0^\infty dv\, v \cos\theta\, n_v(v) \int_0^\infty dm\, m\, n_m(m) \qquad (48)$$

$$mv_\perp = \frac{2}{3} m_T \langle v \rangle$$

$$mv_\perp \doteq 0.3 \text{ dyne - sec/m}^2 \text{ day}$$

or a pressure of 2×10^{-11} N/m^2 which is 10^5 times smaller than radiation pressure.

The energy flux is

$$\dot{E} = \tfrac{1}{2} m_T \langle v^2 \rangle$$

$$E = 4 \times 10^{-2} \text{ Joules/m}^2 \text{ day}$$

which over the entire earth amounts to a power input of 200 megawatts.

COMPARISONS WITH OTHER EXPERIMENTS

It appears that satellite penetration measurements together with radar and photographic observations of meteors yield a consistent picture of the earth's

meteoroid environment. There is considerable disagreement between this picture and the previously accepted meteoroid environment based on collection experiments and acoustical and photomultiplier sensing of impacts from very small meteoroids. This disagreement had been suspected for some time because of the failure of various early experiments using wire grids or similar sensors that required physical damage to detect anywhere near the number of events predicted by the acoustical measurements. The low puncture rate observed by Explorer XVI confirmed this disparity.

As an example of the order of magnitude of this discrepancy, the mass flux relation obtained by Alexander et al [13] from acoustic measurement of the momentum imparted to sounding boards is

$$\log N = -17 - 1.7 \log M$$

where N is the number of encounters per square meter second with meteoroids of mass M or greater. The characteristic mass for the Explorer XVI 0.0025-cm pressure cells is $10^{-9.55}$ gm. From Alexander's results the cells should be punctured at a rate of $10^{-1.5}$ per m^2 second or $10^{3.4}$ per square meter day. This is almost four orders of magnitude higher than what was actually observed. Furthermore, the quantity d log N/d log M is -1.7 according to Alexander's results but was observed to be only -0.3 from the penetration measurements. It is inconceivable that a measurement as straightforward as the Explorer XVI pressure cell experiment could measure four orders of magnitude too low. Most of the cells eventually registered a puncture, which is convincing evidence that the cells retained pressure and therefore were not punctured prior to the indicated time. There appears to be only two possible explanations of this discrepancy; (1) the acoustical data are in serious error, or (2) meteoroids are far less penetrating than expected. Although the empirical penetration formula used to predict characteristic mass for puncture is an extrapolation, it is based on laboratory data which contains the size range in question and velocities well into the meteoroid range (> 10 km/sec). Most of the small mass, high velocity penetration data have been restricted to densities of 1 gm/cm^3 and higher, but theoretical studies [5] indicate high velocity particles of porous Al (0.44 gm/cm^3) are just as penetrating for a given mass as those of normal density. If the acoustical measurements are actually measuring momentum of impacting meteoroids, the only explanation of the failure to observe a large number of penetrations in very thin metallic foils must be a combination of very low relative velocities and extremely tenuous particles. Even if such particles were in geocentric orbits similar to the orbit of the satellite carrying the measurement, the fact that the satellites involved have fairly high inclinations requires the particles to have

relative velocities as high as 8 km/sec, with an average velocity of around 5 km/sec. The low penetration rate observed on the 0.0025-cm Explorer XVI and XXIII pressure cells and the failure to observe any penetrations on Jennison's [4] 0.0012- and 0.0015-cm foils on Ariel II require incredibly low densities. It is clear that to explain both the acoustic measurements and the penetration measurements, it is necessary to assume two distinct families of meteoroids. The mass distribution obtained in this work applies to moderate density, penetrating particles in heliocentric orbits. The slope and magnitude of this distribution is such that a very small fraction of the acoustic events can be attributed to this family. If the acoustic events are actually caused by meteoroid encounters, the particles must belong to a family of extremely tenuous, non-penetrating particles in a distribution whose population declines rapidly with increasing mass. The much smaller decrease in population with mass observed for the family of penetrating particles indicates that an insignificant fraction of observed penetrations can be attributed to the more massive members of the family of non-penetrating particles.

The assumption of this near-earth dust belt whose mass distribution is approximately four orders of magnitude higher than the interplanetary background raises a major theoretical objection which has not been resolved despite considerable efforts on the part of several investigators. Because of their small size and apparent low density, such particles in a near-earth orbit could not remain indefinitely because of radiation perturbations. Therefore, they must somehow be supplied. An extensive analysis of possible concentration mechanisms was performed in which no means of providing a concentration of dust in the vicinity of the earth to the extent implied by the acoustic measurements was found. [1]

The difficulties encountered in attempting to explain the existence of such a near-earth concentration of dust as well as the peculiar properties that must be ascribed to such dust particles to account for their failure to penetrate very thin metallic foils demand that the evidence for their existence be reevaluated. The bulk of this evidence has been supplied by acoustical measurements. It has recently been demonstrated that certain types of acoustical impact measuring devices are susceptible to noise during thermal cycling. [2, 3] This could account for the fact that acoustical detectors operating in the vicinity of earth where they traverse the earth's shadow exhibit a high count rate while the same detectors operating in a fairly constant thermal environment on space probes give results

1. Shapiro, I.I.; Lautman, D.A.; and Colombo, G.: The Earth's Dust Belt: Fact or Fiction. J. Geophys. Res. (to be published).

2. Private discussions with personnel at Langley Research Center, Sept. 1965.

3. Nilsson, C.: Some Doubts about the Earth's Dust Cloud. Science (to be published).

reasonably consistent with estimates based on penetration experiments and zodiacal light studies. However, there is still the unexplained fact that collection experiments flown on satellites as well as rocket probes have returned a very large number of particles, some of which were collected undamaged.

It is clear that there are still many unanswered questions that must be resolved before all of the above measurements can be properly interpreted. Since there is some doubt concerning the measurements that imply the large concentration of non-penetrating particles, these data are not used in the present analysis. If these measurements can be verified, and the existence of a near-earth dust belt of extremely tenuous particles is demonstrated, the mass distribution obtained in this present analysis must be modified to include this component. Several challenging problems concerning the origin and nature of such particles must then be solved. It is not considered likely that such a finding will alter the penetration frequency predictions obtained by the present study for thicknesses greater than 0.01 mm aluminum.

CONCLUSIONS

A penetrating flux model has been developed by essentially extrapolating the Pegasus data to larger and smaller thickness using slopes d log N/d log M determined from ground based and other satellite penetration measurements. The major source of uncertainty lies in the functional relations of mass to penetration and of mass to peak photographic magnitude. A secondary source lies in the freedom of choices in the representation of these slopes as a function of cumulative flux. This freedom can be restricted substantially by additional radar or photographic measurements of this log derivative from $N = 10^4$ to 10^6 per m^2 day steradian, i.e., between Elford's data and the Super-Schmidt data. Such measurements can certainly be made and perhaps already exist, but have not been reported in a form amenable to this analysis. As for the uncertainties in the mass relation, the problem arises because the empirical values for the mass exponent differ from those embodied in the theoretical models. Therefore, some uncertainty exists until the reasons for these differences are understood.

A "best fit" cumulative mass flux has been found to within a constant of integration without having to specify the mass involved in any observation. A constant of integration was calculated for each measurement by estimating a value for the mass (having average velocity, average density, and normal incidence) characteristic to the observation. The average of these constants was used in the "best fit" mass flux.

The mass distribution function was obtained from the cumulative mass flux and is found to agree remarkably well with the interplanetary dust distribution derived by Van de Hulst from interpretation of photometric measurements of F-corona and zodiacal light. Also it was found that interplanetary measurements of dust by Alexander on Mariner IV were in order of magnitude agreement. These results suggest that the environment is not substantially different in interplanetary space. Also the fact that the slopes determined from satellite penetration data appear to rapidly approach zero as N increases, suggests an upper limit on the number of meteoroid encounters which appears to be on the order of $3/m^2$ day regardless of size. This low value is consistent with the fact that only one discernable impact crater was found on a Gemini window. This also suggests that erosion from meteoroids is insignificant and that puncture rate in thin materials is far less than earlier estimates. This low value for the maximum encounter frequency demands that a meaningful meteoroid experiment must expose an area on the order of a m^2 to collect a good statistical sample in a reasonable time.

There is a possibility that there exists, in addition to the family of meteoroids treated in this study, a very large population of particles concentrated near-earth that for some reason are not able to penetrate materials as thin as 0.01 mm aluminum. How such a concentration could exist and how the particles in this family could have such low penetrating power are not understood. Until the existence of this family is more conclusively demonstrated, it will not be considered. Even if this family does exist, the low penetrating ability of its consistent particles must be such that it will not contribute significantly to the meteoroid hazard estimates presented in this paper.

REFERENCES

1. Dohnanyi, J.S.: Model Distribution of Photographic Meteors. Bellcomm TR-66-340-1, March 29, 1966.

2. Jacchia, L. G.; Verniani, F.; and Briggs, R. E.: Smithsonian Special Report No. 175, April 23, 1965.

3. Verniani, F. and Hawkins, G. S.: Masses, Magnitudes, and Densities of 320 Radio Meteors. Harvard Radio Meteor Project Research Report No. 12, March 1965.

4. Payne, J. J.: Impacts of Spherical Projectiles of Aluminum, Stainless Steel, Titanium, and Lead into Semi-infinite Targets of Aluminum and Stainless Steel. AEDC-TR-65-34, Arnold Air Force Station, Tennessee, February 1965.

5. Bjork, R. L.: Final Report. NASW-805 Shock Hydrodynamics, Inc., Sherman Oaks, California, 1966.

6. D'Aiutolo, C. T.: Review of Meteoroid Environment Based on Results from Explorer XIII and Explorer XVI Satellites. Fourth International Space Science Symposium of COSPAR, Warsaw, Poland, June 1963.

7. O'Neal, R. L.: NASA TM X-1123 August 1965.

8. Elford, W. G.: Calculation of the Response Function of the Harvard Radio Meteor Project Radar System. Radio Meteor Project Research Report No. 8, October 1964.

9. Verniani, F.; and Hawkins, G. S.: On the Ionizing Efficiency of Meteors. Harvard Radio Meteor Project Research Report No. 5, February 1964.

10. Hawkins, G. S.; and Upton, E. K. L.: The Influx Rate of Meteors in the Earth's Atmosphere. Astrophys. J., Vol. 128, pp. 727-735, 1958.

11. Van de Hulst, H. C.: Zodiacal Light in the Solar Corona. Astrophys. J., Vol. 105, pp. 471-488, 1947.

REFERENCES (Concluded)

12. Alexander, W. M.; McCracken, C. W.; and Bohn, J. L.: Zodiacal Dust: Measurements by Mariner IV. Science, Vol. 149, pp. 1240-1241, 1965.

13. McCracken, C. W.; and Alexander, W. M.: Direct Measurements of Interplanetary Dust Particles in the Vicinity of Earth. NASA TN D-1174, December 1961.

14. Jennison, R. C.; and McDonnell, J. A. M.: Interpretation of the Interplanetary Dust Measurements in the Ariel II Satellite. Presented at the International Symposium on Meteor Orbits and Dust. Cambridge, Mass., August 1965.

"The aeronautical and space activities of the United States shall be conducted so as to contribute . . . to the expansion of human knowledge of phenomena in the atmosphere and space. The Administration shall provide for the widest practicable and appropriate dissemination of information concerning its activities and the results thereof."

—NATIONAL AERONAUTICS AND SPACE ACT OF 1958

NASA SCIENTIFIC AND TECHNICAL PUBLICATIONS

TECHNICAL REPORTS: Scientific and technical information considered important, complete, and a lasting contribution to existing knowledge.

TECHNICAL NOTES: Information less broad in scope but nevertheless of importance as a contribution to existing knowledge.

TECHNICAL MEMORANDUMS: Information receiving limited distribution because of preliminary data, security classification, or other reasons.

CONTRACTOR REPORTS: Technical information generated in connection with a NASA contract or grant and released under NASA auspices.

TECHNICAL TRANSLATIONS: Information published in a foreign language considered to merit NASA distribution in English.

TECHNICAL REPRINTS: Information derived from NASA activities and initially published in the form of journal articles.

SPECIAL PUBLICATIONS: Information derived from or of value to NASA activities but not necessarily reporting the results of individual NASA-programmed scientific efforts. Publications include conference proceedings, monographs, data compilations, handbooks, sourcebooks, and special bibliographies.

Details on the availability of these publications may be obtained from:

SCIENTIFIC AND TECHNICAL INFORMATION DIVISION

NATIONAL AERONAUTICS AND SPACE ADMINISTRATION

Washington, D.C. 20546